Shaping binary metal nanocrystals through epitaxial seeded growth

SUSAN E. HABAS[1,2], HYUNJOO LEE[1,2], VELIMIR RADMILOVIC[2], GABOR A. SOMORJAI[1,2] AND PEIDONG YANG[1,2]*

[1]Department of Chemistry, University of California, Berkeley, Berkeley, California 94720, USA
[2]Materials Sciences Division, Lawrence Berkeley National Laboratory, 1 Cyclotron Road, Berkeley, California 94720, USA
*e-mail: p_yang@berkeley.edu

Published online: 8 July 2007; doi:10.1038/nmat1957

Morphological control of nanocrystals has become increasingly important, as many of their physical and chemical properties are highly shape dependent. Nanocrystal shape control for both single- and multiple-material systems, however, remains empirical and challenging. New methods need to be explored for the rational synthetic design of heterostructures with controlled morphology. Overgrowth of a different material on well-faceted seeds, for example, allows for the use of the defined seed morphology to control nucleation and growth of the secondary structure. Here, we have used highly faceted cubic Pt seeds to direct the epitaxial overgrowth of a secondary metal. We demonstrate this concept with lattice-matched Pd to produce conformal shape-controlled core–shell particles, and then extend it to lattice-mismatched Au to give anisotropic growth. Seeding with faceted nanocrystals may have significant potential towards the development of shape-controlled heterostructures with defined interfaces.

Heteroepitaxy in gas-phase deposition has been extensively studied for the development of functional heterostructures and devices. The same degree of control is necessary to fully realize the potential of heterostructure formation in solution. The majority of efforts towards solution-phase heterostructure growth have focused on chalcogenide or oxide interfaces[1–7], or the integration of a metallic component with a chalcogenide or oxide structure[8–15]. Fully metallic heterostructures[12,16,17] with controlled shape and interfaces are less well studied[18–21]. Shape control of individual metallic nanoparticles, on the other hand, has been extensively studied[22–27] and can provide a starting point for the development of shaped heterostructures.

We have focused on the use of faceted metal nanocrystals as nucleation centres for the overgrowth of a secondary metal to obtain shape-controlled metal heterostructures. The effect of seeds on the reduction of metals has been well studied[28,29], but little investigation has been done on the effects of seeding with another material[12,30,31]. Here, Pt nanocubes (13.4 nm face diagonal with 13% distribution, 9.5 nm edge length, see Supplementary Information, Fig. S1)[32] were used as seeds for the reduction of K_2PdCl_4 by ascorbic acid in an aqueous surfactant solution (tetradecyltrimethylammonium bromide, TTAB). The epitaxial overgrowth of Pd on these Pt nanocubes gave Pt/Pd bimetallic core–shell cubes (~75%, 37.2 nm face diagonal with 8% distribution, 26.5 nm edge length). The scanning electron microscopy (SEM) image in Fig. 1a shows the overall cubic morphology and monodispersity. The transmission electron microscopy (TEM) image of the array in Fig. 1b clearly shows that there is a single cubic Pt seed at the centre of each core–shell heterostructured nanocube. The X-ray diffraction (XRD) pattern collected on these core–shell nanocubes can be indexed to a face-centred-cubic lattice, as Pd and Pt have a small lattice mismatch of only 0.77% that cannot be resolved by our diffractometer. In the absence of seeds, no shape control was observed; instead, a mixture of large particles (>100 nm), including non-polyhedral particles, rods and various faceted particles, was formed (see Supplementary Information, Fig. S2a). Therefore, the cubic Pt seeds serve two purposes here: they provide a well-defined surface for the overgrowth of the secondary metal and dictate the final shape of the core–shell heterostructures.

Visualizing the orientation of the cubic Pt seed within the cubic Pd shell as well as understanding the nature of the bimetallic interface is difficult for the fully embedded structure in which both components exhibit high contrast by traditional TEM imaging. We used high-angle annular dark-field scanning transmission electron microscopy (HAADF-STEM) to analyse the orientation of the two substructures. Using this method, the Pt cores stand out sharply in relation to the Pd shells owing to the enhanced contrast from the difference in atomic numbers between the two elements (Z-contrast imaging). Figure 1c shows the intense contrast from the Pt cube centred within the Pd shell, which exhibits much lower intensity. Tomographical information, including the mutual orientation of the core and shell, can be extracted from the HAADF-STEM intensity data. Integration of the intensity profile across the face of the Pt/Pd core–shell cubes indicates that the {100} planes of both the Pt core and Pd shell lie at ~90° to one another as expected for the intersection of {100} planes in a cube. We can also see that the Pt cube is oriented with the {100} faces parallel to the {100} faces of the Pd shell as modelled in Fig. 1d. The axes extend along the ⟨100⟩ directions through the {100} faces of the Pt core. Development of the conformal Pd shell occurs early in the reaction, which can be seen by stopping the reaction before reduction is complete. After 5 min of growth, the cubic Pd shell is fully formed but less than 4 nm thick (see Supplementary Information, Fig. S3a,b). Therefore, we can conclude that epitaxial overgrowth of cubic Pd shells on cubic Pt seeds occurs conformally with balanced growth along

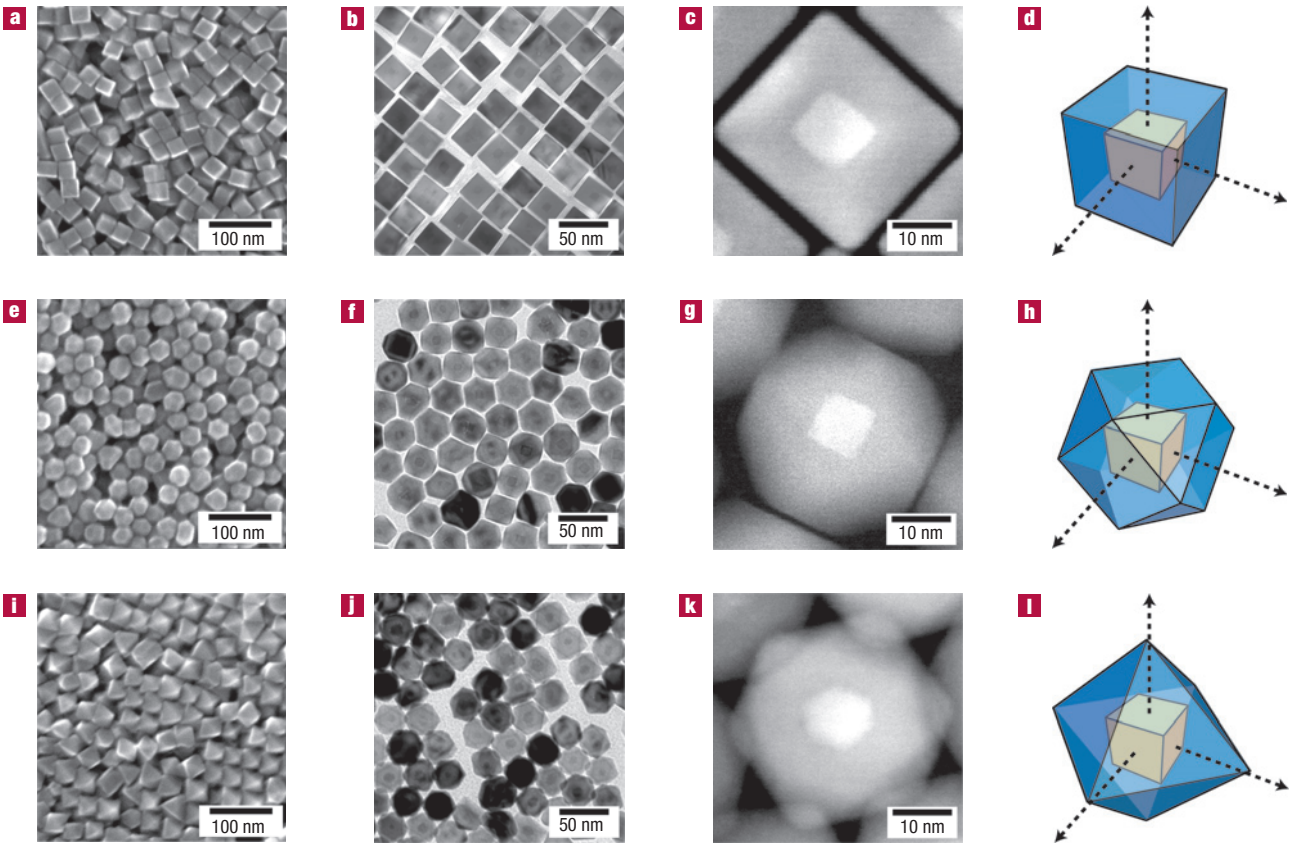

Figure 1 Electron microscopy characterization of the shaped binary metal nanocrystals. Well-defined cubic Pt seeds were used to direct the epitaxial overgrowth of Pd to form Pt/Pd core–shell nanocubes. **a**, The overall morphology is shown by SEM. **b**, TEM indicates the presence of a cubic Pt seed at the core of each particle. **c**, Analysis by HAADF-STEM gives the orientation of the cubic Pt seed within the Pd shell. The Pt core stands out sharply in relation to the Pd shell owing to the enhanced contrast from the difference in atomic numbers between the two elements. **d**, The orientation of the core and shell are modelled with the axes projecting along the ⟨100⟩ directions through the {100} faces of the central Pt cube. **e–l**, Control over the directed growth of Pd on Pt nanocubes was achieved by the addition of increasing amounts of NO_2, which altered the growth rates along the ⟨100⟩ and ⟨111⟩ directions to give Pt/Pd core–shell cuboctahedra (**e–h**) and octahedra (**i–l**). The SEM images (**e**,**i**) are provided for clarification of the three-dimensional morphology, and TEM images (**f**,**j**) to show the presence of a Pt seed at the core of each particle. HAADF-STEM images give the orientation of the cubic Pt seed within a Pd cuboctahedron (**g**) and octahedron (**k**). The Pt/Pd octahedron (**k**) is oriented along the ⟨111⟩ zone axis with the Pt seed on a three-fold axis giving a hexagonal projection. The corresponding models are provided (**h**,**l**).

the ⟨100⟩ and ⟨111⟩ directions from the {100}-terminated cubic Pt seeds.

To understand the epitaxial nature of the core–shell interface within the Pt/Pd nanocubes, we have carried out further high-resolution TEM (HRTEM) imaging. The HRTEM image in Fig. 2a shows negligible contrast between the core and the shell of the Pt/Pd cube because of the high degree of alignment on the ⟨100⟩ zone axis (the expected Pt/Pd interface is shown as a dotted line). However, local distortions of the lattice at the buried interface can be extracted by constructing a phase image, and then a moiré image that corresponds to the positions of the atomic planes. The moiré images in Fig. 2b,c were constructed from the phase images obtained using the (002) and (020) reflections in the Fourier transform of the HRTEM image in Fig. 2a. Analysis of the moiré images indicates that the Pt/Pd interface is fully coherent and epitaxial without observable defects. Both the (002) and (020) constructions show parallel phase intensities extending through the expected Pt/Pd boundaries of the core without exhibiting any displacement. Distortions of the patterns occur in the lower left quadrant of Fig. 2b and the top of Fig. 2c but are not associated with the interfacial region and are probably a result of local surface damage and/or contamination.

Our understanding of the overgrowth process and the epitaxial interface of the Pt/Pd cubes suggests that the defined structure of the Pt seed has a direct influence on the controlled overgrowth of Pd from the epitaxial interface. Extending our control of the directed overgrowth on Pt nanocubes to include shape-control chemistry can allow for the use of the conformal epitaxial growth to produce core–shell particles with other well-defined shapes. Nitrogen dioxide is known to dissociate on Pd surfaces to give adsorbed NO and adsorbed atomic oxygen. The NO desorbs between 230 and 300 K leaving behind adsorbed oxygen[33], which may interact selectively with the Pd surfaces of the growing particles[34]. By adding NO_2, we were able to vary the growth rates along the ⟨100⟩ and ⟨111⟩ directions to give cuboctahedrally (~90%, 36.4 nm body diagonal, with 6% distribution) and octahedrally shaped Pd shells (~90%, 34.6 nm measured two-dimensional projection of the body diagonal with 6% distribution, 40.8 nm calculated body diagonal). The cuboctahedral particles imaged by SEM in Fig. 1e have a more spherical morphology than that shown by TEM (Fig. 1f).

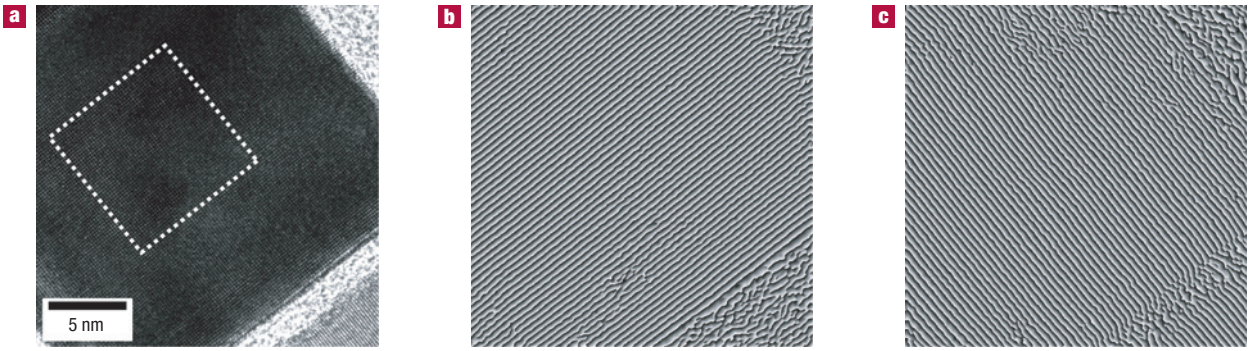

Figure 2 Phase constructions of a Pt/Pd cube showing a coherent and epitaxial interface between the cubic Pt core and Pd shell. a–c, The (002) and (020) reflections from the Fourier transform of the HRTEM image (**a**) were used to construct the corresponding moiré images (**b**,**c**), which indicate that there are no visible distortions through the expected Pt/Pd boundaries, shown by the dotted line in **a**.

A hexagonal projection for particles oriented on their ⟨111⟩ zone axis can be readily seen in Fig. 1f. The SEM image of the octahedra (Fig. 1i) shows particles that are significantly less spherical than the cuboctahedra and have prominent vertices. Analysis by TEM (Fig. 1j) also shows particles that have a hexagonal projection, but unlike the cuboctahedra that pack hexagonally with no overlap, the octahedra overlap at each of their vertices in a manner characteristic of their geometry. The TEM images also show the presence of the Pt seed at the core of each structure.

Here, we have used the decomposition of concentrated HNO_3 in the presence of concentrated HCl (aqua regia) as a NO_2 source, although similar results can be obtained by bubbling NO_2 gas through the reaction to give octahedrally shaped Pt/Pd particles (see Supplementary Information, Fig. S4). For all samples, the acid concentration was kept constant at 1 mM by the addition of HNO_3 to avoid any influence of pH on the reactions containing acidic aqua regia. The addition of aqua regia or NO_2 decreases the reduction rate considerably. Comparative analysis of the ultraviolet–visible spectra for the $[TTA]_2[PdBr_4]$ complex formed before reduction[35], and the complex following exposure to NO_2(g), shows a shift in the absorption maxima from 341 and 252 nm, to 320 nm with a shoulder at 250 nm after NO_2 exposure. This process also corresponds to a colour change from orange to bright yellow. Excessive NO_2 exposure renders the complex incapable of reduction under the conditions used here. As the Pd precursor is reduced, the NO_2 starts to interact with the surfaces of the growing particle. A preferential interaction of NO_2 with the {111} surfaces may act to partially passivate the {111} surfaces with adsorbed oxygen, limiting growth along the ⟨111⟩ directions possibly by altering the interaction of the TTAB surfactant or bromide counterions with the surfaces[36]. As a result, the nanocrystals formed in the presence of 0.1 mM aqua regia (Fig. 1g) exhibit increased growth along the ⟨100⟩ directions. The resulting cuboctahedral shells are partially terminated by {111} planes as shown in Fig. 1h. Analysis of the HAADF-STEM intensity profile across the body diagonal gives a 123.1° angle between the {111} and {100} planes, which agrees well with the expected 125.3° angle. Increasing the amount of aqua regia to 1 mM allows growth along the ⟨100⟩ directions to dominate, giving Pd octahedral shells composed entirely of {111} faces (Fig. 1k,l). The Pt/Pd octahedron in Fig. 1k is oriented along the ⟨111⟩ zone axis with the Pt seed on a three-fold axis giving a hexagonal projection. Halting the reaction before reduction is complete once again shows that overgrowth is epitaxial and conformal, and that growth along the ⟨100⟩ direction to give {111} faces already dominates at an early stage for samples containing NO_2 (see Supplementary Information, Fig. S3c,d). Overgrowth of Pd on small spherical Pt seeds (3.5 nm) in the presence of HNO_3 (see Supplementary Information, Fig. S2b) or aqua regia (see Supplementary Information, Fig. S2c), under conditions that are otherwise the same, does not produce the Pt/Pd cubes or octahedra as described above. Therefore, the uniform {100} surface of the seeds enables precise control of the Pd overgrowth direction to give shells of a defined shape.

It is well known that lattice mismatch has a significant impact on the epitaxial growth of heterostructures for gas-phase deposition. For heterostructures with a high degree of lattice mismatch, the resulting interface is often non-coherent with a large density of defects. Here, we extend the epitaxial overgrowth on cubic Pt seeds to a metal with a larger lattice mismatch. The reduction of Au on cubic Pt seeds (4.08% mismatch versus 0.77% for Pt/Pd) results in the formation of anisotropic rods (~185 nm length and ~25 nm diameter) shown by SEM in Fig. 3a with the high-resolution inset showing the presence of a Pt seed on each rod. Other products in the sample included faceted particles with a seed partially embedded at the perimeter, and twinned particles that initially formed on a facet of the Pt nanocube and then grew to encompass the Pt seed. It is clear that the high lattice mismatch effectively prevents conformal overgrowth on the Pt nanocubes, instead giving heterostructures in which both the seed and the secondary metal are exposed.

We believe that the lattice mismatch rather than the size of the seed gives rise to the non-conformal growth. For example, studies on the effect of Au seed size on Au rod growth have demonstrated the evolution of rods from seeds as large as 18 nm that are presumably encompassed within the rod[29]. Here, however, we have shown anisotropic growth to form Au rods, each containing a single partially embedded Pt cube at the perimeter of the rod (Fig. 3b,c). Following the nucleation of Au on the Pt cube, growth occurs on the high-energy Au nucleate, rather than on the Pt seed, as a result of its smaller size and twinning defects. Further growth occurs bi-directionally, resulting in a Pt/Au structure in which both metals are exposed. Reduction does not occur in the absence of seeds, and Au rods produced from smaller spherical Pt seeds (3.5 nm) probably have seeds enclosed within the rod structure[31]. The Au rods here are also pentagonally twinned as can be seen from the HRTEM image in Fig. 3d showing a Au rod viewed down the ⟨112⟩/⟨100⟩ zone with continuous {111} fringes running parallel to the long axis. The corresponding selected-area electron diffraction pattern (inset) is indicative of a ⟨112⟩ zone

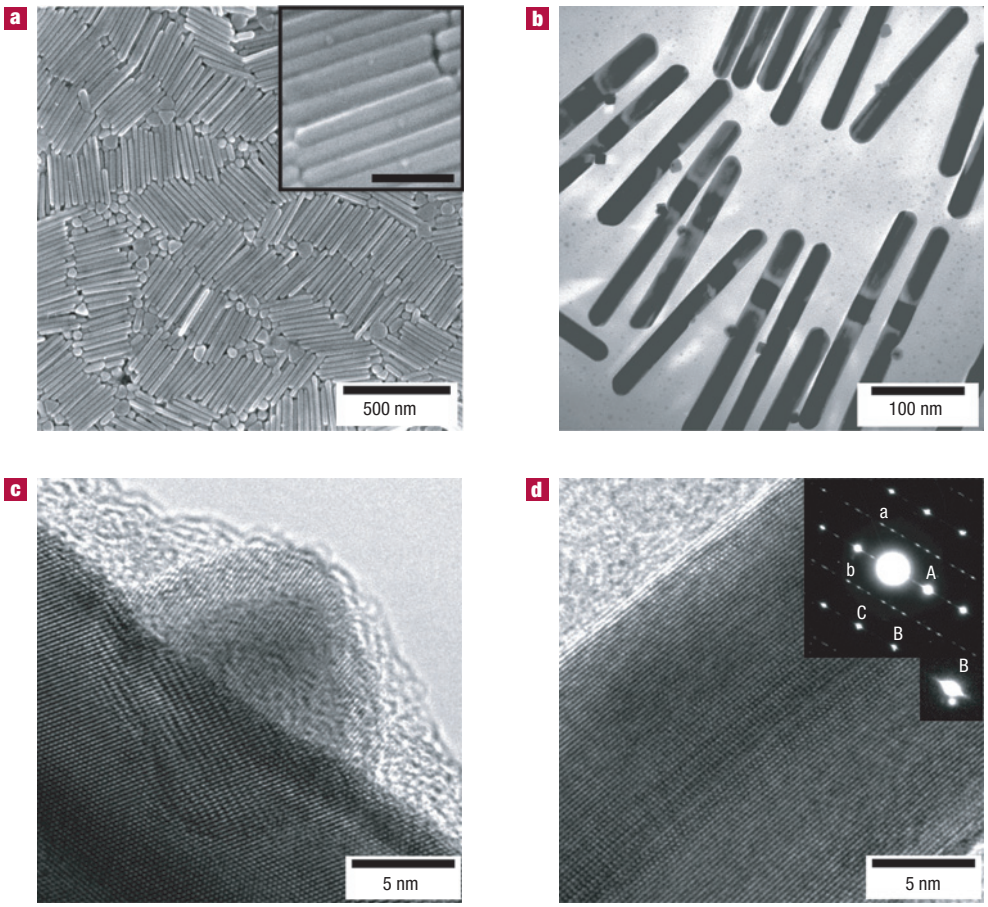

Figure 3 Epitaxial overgrowth of lattice-mismatched Au on cubic Pt seeds to give anisotropic growth of Au rods. a, SEM image showing an overview of Au rods nucleated from cubic Pt seeds, magnified in the inset (the scale bar is 100 nm). **b**, TEM image of multiple rods indicating that a single Pt cube is associated with each Au rod. **c**, HRTEM image showing a single Pt cube partially embedded in the side of a Au rod. **d**, The length of the rod, viewed down the ⟨112⟩/⟨100⟩ zone with continuous {111} fringes running parallel to the long axis, and the corresponding selected-area electron diffraction pattern (inset, discussed in text) with double diffraction is indicative of a pentagonally twinned particle. The magnified view of the $(1\bar{3}1)$ reflection (B) shows a further reflection arising from the Pt cube epitaxially oriented with one of the five [112] zones of the Au rod.

overlapped with ⟨100⟩ zone. The first-order reflections labelled A, B and C correspond to the $(1\bar{1}1)$, (131) and (220) planes of the rectangular $[\bar{1}12]$ reciprocal lattice, and those labelled a, b and C, to the $(\bar{2}00)$, (020) and (220) planes of the square [001] lattice[37]. In addition to the associated double-diffraction reflections, a second smaller set of diffraction spots slightly offset from the Au $[\bar{1}12]$ zone (Fig. 3d, B expanded below inset) can be indexed to the Pt cube epitaxially oriented with one of the five domains of the Au rod.

Shape control enabled by this epitaxial seeding concept allows us to study surface-dependent properties such as catalytic activity. Electrochemical oxidation of formic acid was used to evaluate the catalytic properties of the Pt/Pd core–shell nanocrystals. The effect of surface structure on electrocatalytic activity and selectivity has been extensively studied[38,39]. Both activity and selectivity depend on how the arrangement of atoms at the surface and the corresponding surface energy affects adsorption, surface diffusion, intermediate formation, chemical rearrangements and finally desorption of the products. Structural effects on formic acid oxidation were investigated on single-crystalline Pd electrodes including Pd(100) and Pd(111) (refs 40,41). According to Baldauf and Kolb[40], the Pd(100) single-crystal surface showed an anodic peak current approximately four times higher than that for the Pd(111) surface, which corresponds to an increased oxidation rate of formic acid at the Pd(100) surface. However, the Pd(111) surface gave a lower peak potential (0.07 V versus Ag/AgCl) than the Pd(100) surface (0.42 V) for formic acid oxidation. The Pd(100) single-crystalline electrode was also found to be more susceptible to oxidation than the Pd(111) electrode. Figure 4 shows cyclic voltammograms for formic acid oxidation on Pt/Pd cubes (Fig. 4a), cuboctahedra (Fig. 4b) and octahedra (Fig. 4c). The Pt/Pd cubes show a peak current that is five times higher than that observed for the Pt/Pd octahedra, whereas the octahedra have a lower peak potential (0.15 V) than the cubes (0.36 V). The Pt/Pd cubes also have a sharper peak in the negative scan than the octahedra, at 0.47 V, corresponding to the reduction of Pd oxide. The Pt/Pd cuboctahedra exhibit properties intermediate between the cubes and octahedra.

In summary, we have demonstrated that by controlling the epitaxial overgrowth of a secondary metal on well-faceted cubic Pt seeds, we can produce both conformal shape-controlled overgrowth as well as anisotropic overgrowth depending on the degree of lattice mismatch. This concept could be applied to other material systems (for example, Rh, FePt and CoPt), creating novel heterostructures for catalysis, optical and magnetic applications where shape control plays a crucial role.

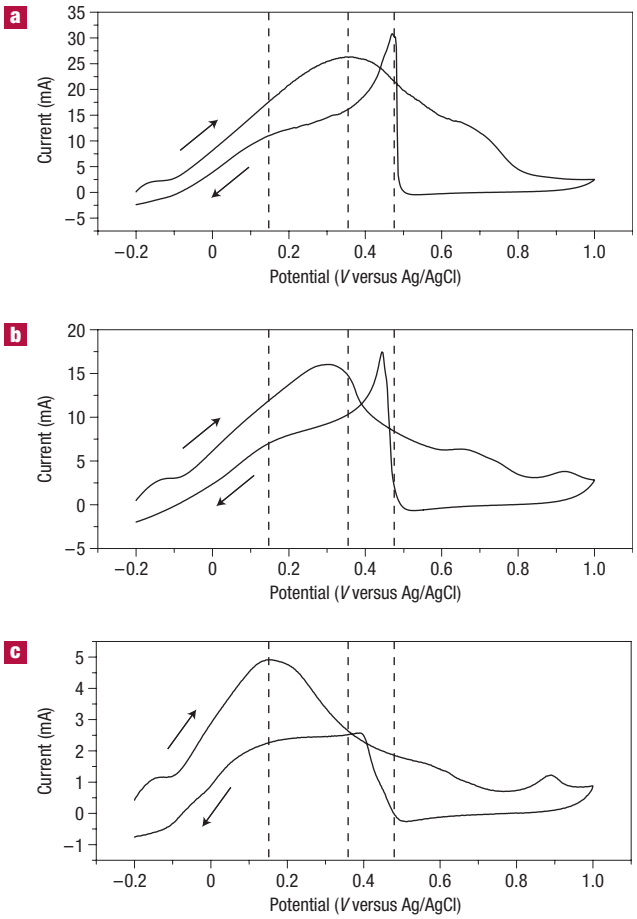

Figure 4 Catalytic activity of the Pt/Pd binary metal nanocrystals. The effect of surface structure on the catalytic activity of the Pt/Pd core–shell nanoparticles was investigated by electrochemical formic acid oxidation. **a–c**, Cyclic voltammograms for cubes (**a**), cuboctahedra (**b**) and octahedra (**c**) were obtained at a sweep rate of 50 mV s^{-1} in 0.1 M H_2SO_4 and 0.2 M formic acid.

METHODS

GROWTH OF Pt SEEDS

Cubic Pt seeds (13.4 nm face diagonal with 13% distribution) were synthesized as described elsewhere[32]. Briefly, 1 mM aqueous K_2PtCl_4 (Aldrich, 99.99%) in 100 mM TTAB was reduced by 30 mM $NaBH_4$ at 50 °C. Excess H_2 evolved from the reaction of water with $NaBH_4$ was released by inserting a needle into the septum capping the reaction vessel. After 6 h, the reaction was allowed to cool to room temperature and left overnight to promote the decomposition of the remaining $NaBH_4$ in water. The Pt nanoparticles were collected after removing larger precipitates by centrifugation. The pH of the seed solution was decreased from ~9 to ~3 to ensure decomposition of residual $NaBH_4$ by the addition of HCl, and then neutralized with NaOH.

Small spherical Pt seeds (3.5 nm) were also prepared according to a method described previously[42]. Reduction of $H_2PtCl_6{\cdot}6H_2O$ (0.6 mM, 99.9%, Alfa Aesar) in an aqueous solution of Pluronic L64 ($EO_{13}PO_{30}EO_{13}$, BASF) triblock copolymer (6 mM, 10 ml) was achieved by the addition of $NaBH_4$ (1 mg) while stirring at room temperature in a closed vial. The reaction was left overnight before use.

EPITAXIAL OVERGROWTH AND SHAPE CONTROL OF Pd SHELLS

Conformal overgrowth of Pd on cubic Pt seeds was achieved by introducing Pt seeds (100 μl) and L-ascorbic acid (50 μl of 100 mM solution) into an aqueous solution (5 ml) containing 100 mM TTAB and 0.5 mM K_2PdCl_4 (Alfa Aesar, 99.99%) that had been heated at 50 °C for 5 min while stirring in a capped vial. The morphology of the Pd shell was altered by increasing the amount of NO_2 added to the reaction conditions described above. This was done either by addition of gaseous NO_2 or a 1:1 volume ratio of HCl (12.1 M) and HNO_3 (15.7 M) (aqua regia) that had been allowed to react for 4 h. The addition of aqua regia in the following concentrations gave cubes (0 mM), cuboctahedra (0.1 mM) and octahedra (1.0 mM). Alternatively, similar results could be obtained by bubbling NO_2 (0.99% in He, Praxair) through H_2O for 30 min and then adding 10 μl of this solution to the reaction to give Pt/Pd octahedra. For all reactions, the total acid concentration was held constant at 1 mM with the difference made up by the addition of HNO_3. All acids and NO_2 were added to the TTAB solution before the Pd salt. Cubic samples were removed from the heat after 1 h, and cuboctahedral and octahedral samples after 2.5 h.

GROWTH OF ANISOTROPIC Au RODS

The Au rods were prepared by adding cubic Pt seeds (25 μl) into a solution (5 ml) containing 100 mM TTAB, 0.25 mM $HAuCl_4$ (99.9%, Alfa Aesar) and 0.5 mM L-ascorbic acid. The solution was shaken briefly in a capped vial, and Au reduction was indicated by the development of a pale pink colour within 30 s. Reduction was allowed to proceed for at least 5 min to give a deep purple/pink solution. Reactions were carried out at room temperature owing to the fast reduction of Au by ascorbic acid in the presence of seeds.

ELECTROCATALYTIC FORMIC ACID OXIDATION

Electrochemical measurements were carried out in 0.1 M H_2SO_4 and 0.2 M formic acid at room temperature. A three-electrode cell was used with a Ag/AgCl reference electrode and a gold wire as the counter electrode. The Pt/Pd core–shell nanoparticles (10 ml) were washed and concentrated to 0.1 ml then deposited on a gold-foil working electrode and dried for 2 h. Cyclic voltammetry data were collected at a sweep rate of 50 mV s^{-1} after stabilizing the cyclic voltammetry curve through repetitive scans that acted to remove surfactant molecules from the Pd surfaces.

SAMPLE CHARACTERIZATION

The structure and composition of the samples were investigated by XRD (Co Kα radiation, D-8 GADDS general area detector, Bruker), SEM (FEI Strata 235 Dual Beam FIB), TEM (JEOL 200CX and Tecnai G^2 S-Twin), HRTEM (Philips, CM200) and HAADF-STEM (FEI monochromated F20 UT Tecnai). Samples were centrifuged and washed with fresh TTAB solution and then water before resuspending in water and drying on a silicon substrate for XRD and SEM, or a carbon-coated copper grid for TEM.

Received 23 April 2007; accepted 18 June 2007; published 8 July 2007.

References

1. Milliron, D. J. *et al.* Colloidal nanocrystal heterostructures with linear and branched topology. *Nature* **430**, 190–195 (2004).
2. Kudera, S. *et al.* Selective growth of PbSe on one or both tips of colloidal semiconductor nanorods. *Nano Lett.* **5**, 445–449 (2005).
3. Buonsanti, R. *et al.* Seeded growth of asymmetric binary nanocrystals made of a semiconductor TiO_2 rodlike section and a magnetic γ-Fe_2O_3 spherical domain. *J. Am. Chem. Soc.* **128**, 16953–16970 (2006).
4. Talapin, D. V. *et al.* Highly emissive colloidal CdSe/CdS heterostructures of mixed dimensionality. *Nano Lett.* **3**, 1677–1681 (2003).
5. Kwon, K.-W. & Shim, M. γ-Fe_2O_3/II-VI sulfide nanocrystal heterojunctions. *J. Am. Chem. Soc.* **127**, 10269–10275 (2005).
6. Kwon, K.-W., Lee, B. H. & Shim, M. Structural evolution in metal oxide/semiconductor colloidal nanocrystal heterostructures. *Chem. Mater.* **18**, 6357–6363 (2006).
7. Teranishi, T., Inoue, Y., Nakaya, M., Oumi, Y. & Sano, T. Nanoacorns: Anisotropically phase-segregated CoPd sulfide nanoparticles. *J. Am. Chem. Soc.* **126**, 9914–9915 (2004).
8. Mokari, T., Sztrum, C. G., Salant, A., Rabani, E. & Banin, U. Formation of asymmetric one-sided metal-tipped semiconductor nanocrystal dots and rods. *Nature Mater.* **4**, 855–863 (2005).
9. Shi, W. *et al.* A general approach to binary and ternary hybrid nanocrystals. *Nano Lett.* **6**, 875–881 (2006).
10. Yu, H. *et al.* Dumbbell-like bifunctional Au-Fe_3O_4 nanoparticles. *Nano Lett.* **5**, 379–382 (2005).
11. Gu, H., Zheng, R., Zhang, X. & Xu, B. Facile one-pot synthesis of bifunctional heterodimers of nanoparticles: A conjugate of quantum dot and magnetic nanoparticles. *J. Am. Chem. Soc.* **126**, 5664–5665 (2004).
12. Gu, H., Yang, Z., Gao, J., Chang, C. K. & Xu, B. Heterodimers of nanoparticles: Formation at a liquid-liquid interface and particle-specific surface modification by functional molecules. *J. Am. Chem. Soc.* **127**, 34–35 (2005).
13. Yang, J., Elim, H. I., Zhang, Q., Lee, J. Y. & Ji, W. Rational synthesis, self-assembly, and optical properties of PbS-Au heterogeneous nanostructures via preferential deposition. *J. Am. Chem. Soc.* **128**, 11921–11926 (2006).
14. Casavola, M. *et al.* Topologically controlled growth of magnetic-metal-functionalized semiconductor oxide nanorods. *Nano Lett.* **7**, 1386–1395 (2007).
15. Pacholski, C., Kornowski, A. & Weller, H. Nanomaterials: Site-specific photodeposition of silver on ZnO nanorods. *Angew. Chem. Int. Edn* **43**, 4774–4777 (2004).
16. Pellegrino, T. *et al.* Heterodimers based on $CoPt_3$-Au nanocrystals with tunable domain size. *J. Am. Chem. Soc.* **128**, 6690–6698 (2006).

17. Gao, X., Yu, L., MacCuspie, R. I. & Matsui, H. Controlled growth of Se nanoparticles on Ag nanoparticles in different ratios. *Adv. Mater.* **17**, 426–429 (2005).
18. Xiang, Y. *et al*. Formation of rectangularly shaped Pd/Au bimetallic nanorods: Evidence for competing growth of the Pd shell between the {110} and {100} side facets of Au nanorods. *Nano Lett.* **6**, 2290–2294 (2006).
19. Krichevski, O., Tirosh, E. & Markovich, G. Formation of gold-silver nanowires in thin surfactant solution films. *Langmuir* **22**, 867–870 (2006).
20. Tsuji, M. *et al*. Crystal structures and growth mechanisms of Au@Ag core–shell nanoparticles prepared by the microwave-polyol method. *Cryst. Growth Des.* **6**, 1801–1807 (2006).
21. Sanedrin, R. G., Georganopoulou, D. G., Park, S. & Mirkin, C. A. Seed-mediated growth of bimetallic prisms. *Adv. Mater.* **17**, 1027–1031 (2005).
22. Kim, F., Connor, S., Song, H., Kuykendall, T. & Yang, P. Platonic gold nanocrystals. *Angew. Chem. Int. Edn* **43**, 3673–3677 (2004).
23. Song, H., Kim, F., Connor, S., Somorjai, G. A. & Yang, P. Pt nanocrystals: Shape control and Langmuir-Blodgett monolayer formation. *J. Phys. Chem. B* **109**, 188–193 (2005).
24. Tao, A., Sinsermsuksakul, P. & Yang, P. Polyhedral silver nanocrystals with distinct scattering signatures. *Angew. Chem. Int. Edn* **45**, 4597–4601 (2006).
25. Chen, J., Herricks, T. & Xia, Y. Polyol synthesis of platinum nanostructures: Control of morphology through the manipulation of reduction kinetics. *Angew. Chem. Int. Edn* **44**, 2589–2592 (2005).
26. Sau, T. K. & Murphy, C. J. Room temperature, high-yield synthesis of multiple shapes of gold nanoparticles in aqueous solution. *J. Am. Chem. Soc.* **126**, 8648–8649 (2004).
27. Wiley, B., Sun, Y., Mayers, B. & Xia, Y. Shape-controlled synthesis of metal nanostructures: The case of silver. *Chem. Eur. J.* **11**, 454–463 (2005).
28. Murphy, C. J. & Jana, N. R. Controlling the aspect ratio of inorganic nanorods and nanowires. *Adv. Mater.* **14**, 80–82 (2002).
29. Gole, A. & Murphy, C. J. Seed-mediated synthesis of gold nanorods: Role of the size and nature of the seed. *Chem. Mater.* **16**, 3633–3640 (2004).
30. Yong, K.-T. *et al*. Shape control of PbSe nanocrystals using noble metal seed particles. *Nano Lett.* **6**, 709–714 (2006).
31. Sun, Y., Yin, Y., Mayers, B. T., Herricks, T. & Xia, Y. Uniform silver nanowires synthesis by reducing $AgNO_3$ with ethylene glycol in the presence of seeds and poly(vinyl pyrrolidone). *Chem. Mater.* **14**, 4736–4745 (2002).
32. Lee, H. *et al*. Morphological control of catalytically active platinum nanocrystals. *Angew. Chem. Int. Edn* **45**, 7824–7828 (2006).
33. Banse, B. A. & Koel, B. E. Interaction of oxygen with palladium(111): High effective oxygen pressure conditions by using nitrogen dioxide. *Surf. Sci.* **232**, 275–285 (1990).
34. Somorjai, G. A. *Introduction to Surface Chemistry and Catalysis* (Wiley, New York, 1994).
35. Veisz, B. & Kiraly, Z. Size-selective synthesis of cubooctahedral palladium particles mediated by metallomicelles. *Langmuir* **19**, 4817–4824 (2003).
36. Pileni, M.-P. The role of soft colloidal templates in controlling the size and shape of inorganic nanocrystals. *Nature Mater.* **2**, 145–150 (2003).
37. Johnson, C. J., Dujardin, E., Davis, S. A., Murphy, C. J. & Mann, S. Growth and form of gold nanorods prepared by seed-mediated, surfactant-directed synthesis. *J. Mater. Chem.* **12**, 1765–1770 (2002).
38. Lamy, C. & Leger, J. M. Electrocatalytic oxidation of small organic molecules at platinum single crystals. *J. Chim. Phys.* **88**, 1649–1671 (1991).
39. Markovic, N. M. & Ross, P. N. Surface science studies of model fuel cell electrocatalysts. *Surf. Sci. Rep.* **45**, 117–229 (2002).
40. Baldauf, M. & Kolb, D. M. Formic acid oxidation on ultrathin Pd films on Au(*hlk*) and Pt(*hkl*) electrodes. *J. Phys. Chem.* **100**, 11375–11381 (1996).
41. Hoshi, N., Kida, K., Nakamura, M., Nakada, M. & Osada, K. Structural effects of electrochemical oxidation of formic acid on single crystal electrodes of palladium. *J. Phys. Chem. B* **110**, 12480–12484 (2006).
42. Niesz, K., Grass, M. & Somorjai, G. A. Precise control of the Pt nanoparticle size by seeded growth using $EO_{13}PO_{30}EO_{13}$ triblock copolymers as protective agents. *Nano Lett.* **5**, 2238–2240 (2005).

Acknowledgements

This work was supported by the US Department of Energy under Contract #DE-AC02-05CH11231. All TEM investigations, with the exception of those done on the Tecnai G^2 S-Twin, were carried out at the National Center for Electron Microscopy, Lawrence Berkeley National Lab. We would also like to thank T. R. Kuykendall for the SEM work.
Correspondence and requests for materials should be addressed to P.Y.
Supplementary Information accompanies this paper on www.nature.com/naturematerials.

Competing financial interests

The authors declare no competing financial interests.